Electronic Supplementary Information

Mass production of thin-walled hollow optical fibers enables disposable optofluidic laser immunosensors

Xi Yang,[a#] Yanhua Luo,[b#] Yiling Liu,[a] Chaoyang Gong,[ac] Yanqiong Wang,[a] Yun-Jiang Rao,[a] Gang-Ding Peng*[b] and Yuan Gong*[a]

[a] Key Laboratory of Optical Fiber Sensing and Communications (Ministry of Education of China), University of Electronic Science and Technology of China, Chengdu, Sichuan 611731, China

[b] School of Electrical Engineering and Telecommunications, University of New South Wales, Sydney, NSW 2052, Australia

[c] School of Electrical and Electronics Engineering, Nanyang Technological University, 50 Nanyang Ave, Singapore, 639798 Singapore.

#These authors contribute equally to this work.

Corresponding authors:

*Prof. Gang-Ding Peng

Address: MSE Building, School of Electrical Engineering and Telecommunications, University of New South Wales, Sydney, NSW 2052, Australia.

Email: g.peng@unsw.edu.au; Telephone: +61-2-93854014

*Prof. Yuan Gong

Address: No. 2006, Xiyuan Ave., High-Tech Zone (West), Chengdu, Sichuan 611731, China.

Email: ygong@uestc.edu.cn; Telephone: +86-13880938317

I. Relationship between HOF thickness and fiber drawing speed

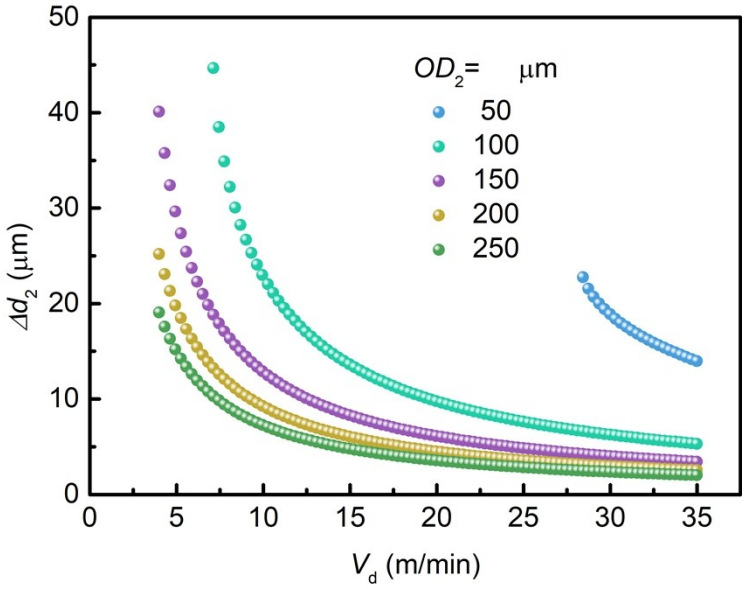

Figure S1 Theoretically calculated HOF thickness Δd_2 versus fiber drawing speed V_d. The results were simulated with different outer diameter of HOF, according to the simplified mass conversation law. In the calculations, OD_1=25 mm, Δd_1=1.5 mm, V_f=0.5 mm/min.

II. Numerical simulation of light distribution

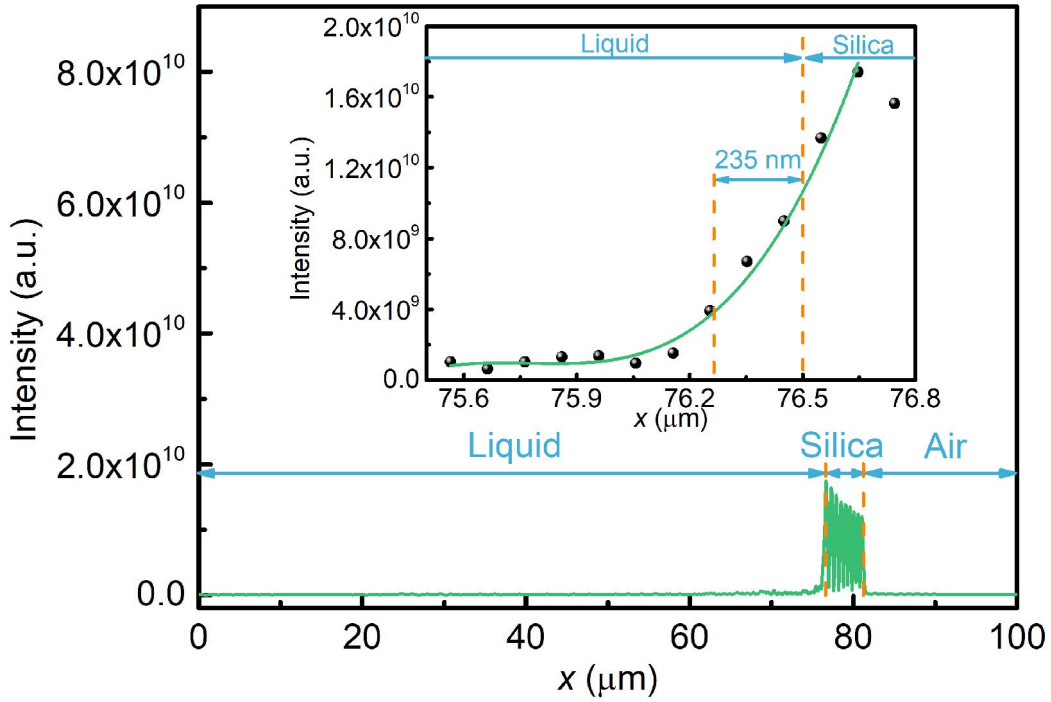

Figure S2 Light intensity along the radial direction of HOF ($x > 0$, $y = 0$). In the inset, the evanescent field distribution indicates a penetration depth of 235 nm.

III. The Q-factor of the HOF microcavity

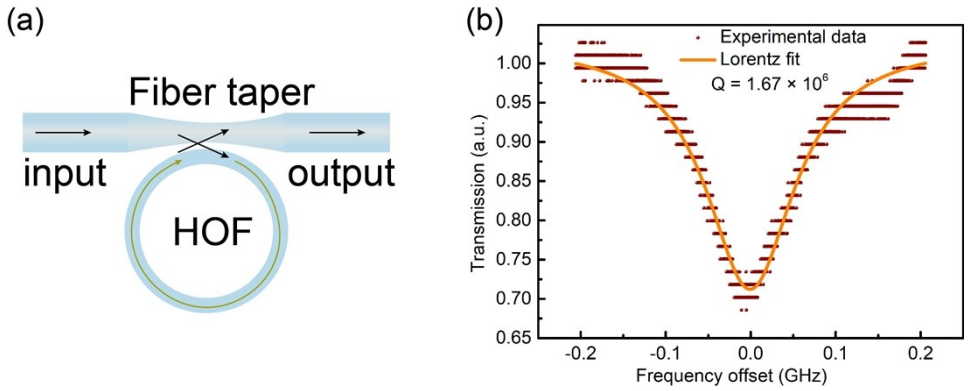

Figure S3 (a) Schematic diagram of the setup for the HOF Q-factor test. (b)The transmission spectrum for the fiber taper-HOF microring resonator system fitted with Lorentz curve. It shows a Q-factor of 1.67×10^6.

IV. Experimental setup for disposable OFL immunosensor

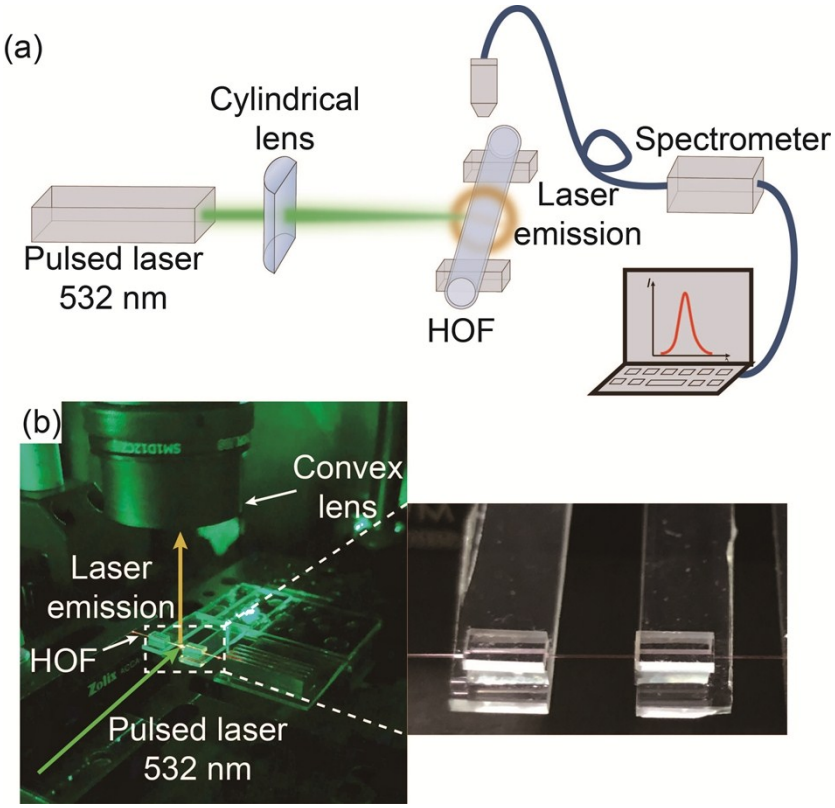

Figure S4 (a) The schematic diagram and (b) photo of the experimental setup for disposable OFL immunosensor. The inset of (b) shows details of the V-shaped grooves for replacing the reproducible HOF during the disposable use.

V. The theoretical model and numerical simulation of the sensing mechanism

A simplified theoretical model is established to analyze the sensing mechanism. The mechanism of scattering loss in the microring resonator is the same as that in the Fabry-Perot (FP) cavity,[1] however, the degree of participation for the gain molecules and the resonance mechanism in those two resonators are different.

In the fiber microring resonator, the laser beam would be scattered by the immune complexes through the Beer-Lambert law,[2]

$$I_R = I_0 e^{-\alpha_s L} \tag{1}$$

where I_R and I_0 are the intensity of the residual light after the scattering and incident light, respectively. α_s is the scattering coefficient (/m). L is the cavity length. Here we ignore the absorption and reflection by the immune complex and only investigate its scattering effect on the optofluidic laser emission.

According to the resonance mechanism of whispering gallery mode (WGM) microresonators, only the light satisfied the total internal reflection (TIR) and phase matching condition can oscillate in the WGM microresonator. The HOF microring resonator achieves TIR at the HOF-air interface when the incident angle is larger than the critical angle (θ_c) calculated to be 43.3° by $\theta_c = \arcsin(n_1 / n_2)$, $n_1 = 1.0$ and $n_2 = 1.46$ the refractive index (RI) of air and HOF, respectively. That is, the maximum incident angle for light to oscillate in microresonator is about 46.7° (Fig. S5a). We further assume that only the scattering light from 0° to 46.7° can couple into

the microring. According to the Rayleigh scattering theory, the scattering light at an angle of θ, with respect to the direction of incident beam, is expressed as:[3]

$$I_\theta = I_0 \frac{8\pi^4 \varepsilon^2}{\lambda_L^4 r^2}(1+\cos^2\theta) \quad (2)$$

$$I_R = \sum_{\theta=0^o}^{\theta_1} I_\theta \quad (3)$$

Here, I_θ is the scattering light at the angle of θ, θ_1=46.7°, ε is the molecular polarizability, λ_L is the optofluidic laser wavelength, and r is the average distance between the immune complexes. The concentration of immune complexes, C_{immuno}, can be simplified and denoted by the concentration of protein, $C_{protein}$, by $C_{immuno} = ktC_{protein}$. Then the average immune complex distance, r, can be estimated to be

$$r = \left(\frac{1}{ktN_A C_{protein}}\right)^{\frac{1}{3}} \quad (4)$$

Here, N_A is the Avogadro constant and t is the immune reaction time. k is a constant coefficient.

The laser intensity changes with the scattering loss according to[4,5]

$$I_{laser} = \frac{\delta_e I_{sat}}{2}\left(\frac{\eta g L}{(\alpha_0 + \eta\alpha_s)L + \delta_e} - 1\right) \quad (5)$$

Here, we introduce a factor, η, as the degree of participation for the gain molecules to participate in lasing. Compared to the conventional FP optofluidic laser, the single-pass gain in the fiber microring resonator is reduced by η. δ_e and g are the external coupling factor of the WGM and unsaturated gain coefficient, respectively. $\alpha_0 = 2\pi n_2 / \lambda_L Q$ denotes the loss of the WGM cavity with λ_L the emission

wavelength, Q the Q-factor of the HOF microring cavity. $I_{sat} = hw/\sigma\tau_{eff}$ is the saturation intensity with h (6.626×10^{-34} J·s) the Planck constant, w the frequency of pump light, σ the fluorophore absorption cross-section, τ_{eff} the effective recovery time of the transition. The numerical simulation results of temporal evolution and sensing curve for optofluidic laser immunosensor are shown in Figs. S5b and S5c, which can qualitatively describe the trend of optofluidic laser immunosensing and is in agreement with the results in Fig. 4.

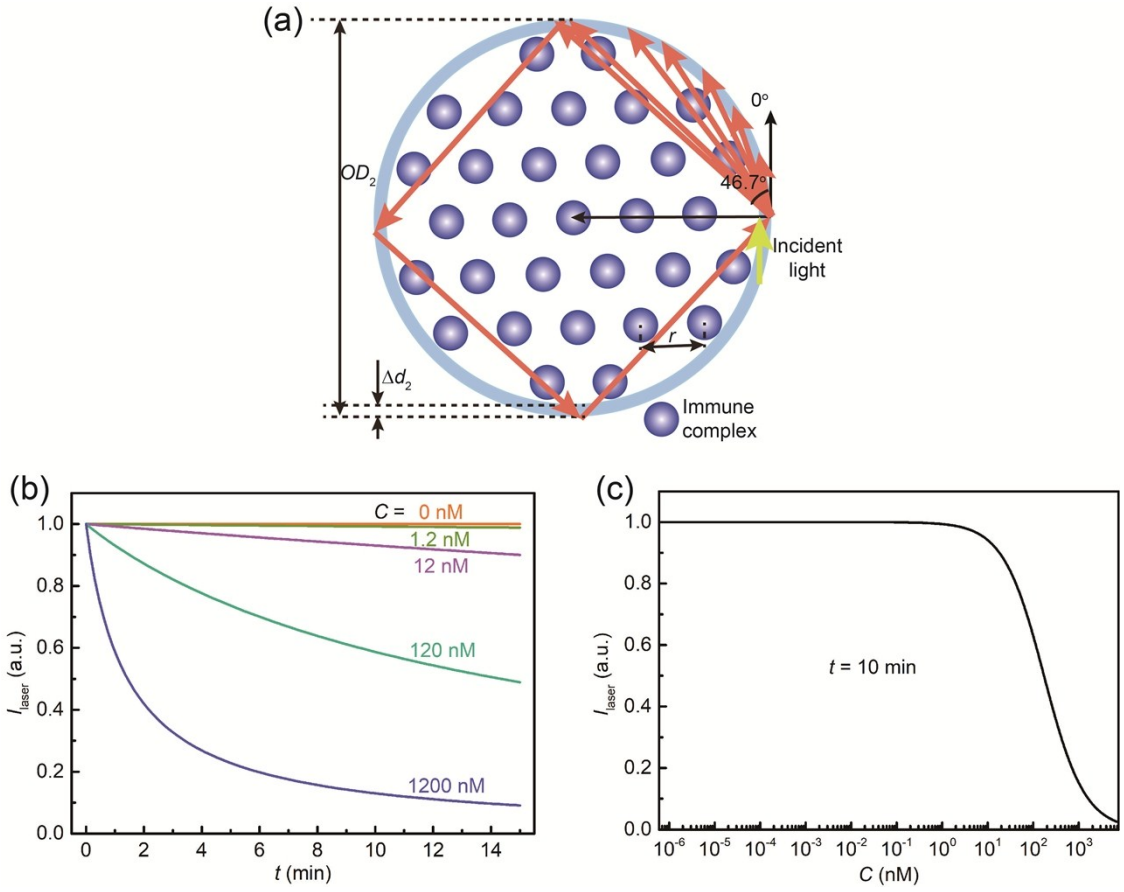

Figure S5 (a) The simplified model for disposable OFL immunosensing, in which the dye molecules and immune complex are uniformly distributed in solution within the HOF. OD_2 and Δd_2 are the outer diameter and thickness of HOF, respectively; r is the average distance between immune complexes. (b) Temporal variation of the

simulated OFL intensity at various protein concentrations. (c) Simulated laser intensity I_{laser} versus protein concentration at a fixed reaction time. In the simulation, I_0 = 1, ε = 13.24 nm^3, λ_L = 600 nm, L = 480.42 μm, k = 10^{-6}, δ_e = 0.01, σ = 6×10^{-16} cm^2, τ_{eff} = 2.6 ns, g = 5×10^5 m^{-1}, n_2 = 1.46, η = 3.22%, and Q = 1.67 × 10^6 are used. This numerical simulation qualitatively reflects the trend for the laser intensity changes with an increasing concentration of protein.

Reference

1 X. Yang, W. Shu, Y. Wang, Y. Gong, C. Gong, Q. Chen, X. Tan, G. D. Peng, X. Fan and Y. J. Rao, *Biosens. Bioelectron.*, 2019, **131**, 60-66.

2 D. F. Swinehart, *J. Chem. Educ.*, 1962, **39**, 333-335.

3 J. T. Whicher, C. P. Price and K. Spencer, *Crit. Rev. Clin. Lab. Sci.*, 1982, **18**, 213-260.

4 A. E. Siegman, *Lasers*, 1986.

5 H. J. Moon, Y. T. Chough and K. An, *Phys. Rev. Lett.*, 2000, **85**, 3161-3164.